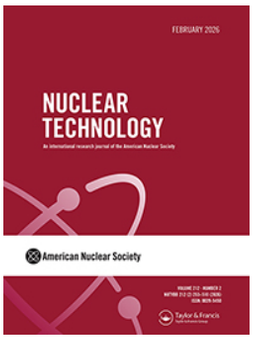

Nuclear Technology

ISSN: 0029-5450 (Print) 1943-7471 (Online) Journal homepage: www.tandfonline.com/journals/unct20

Uncertainty and Sensitivity Analysis of the ASTEC Source Term Results of a MBLOCA Scenario with the Activation of Severe Accident Management Actions in a Generic Konvoi Plant

Anastasia Stakhanova, Fabrizio Gabrielli , Victor Hugo Sanchez Espinoza , Eva-Maria Pauli & Axel Hoefer

To cite this article: Anastasia Stakhanova, Fabrizio Gabrielli , Victor Hugo Sanchez Espinoza , Eva-Maria Pauli & Axel Hoefer (19 Nov 2025): Uncertainty and Sensitivity Analysis of the ASTEC Source Term Results of a MBLOCA Scenario with the Activation of Severe Accident Management Actions in a Generic Konvoi Plant, Nuclear Technology, DOI: 10.1080/00295450.2025.2544372

To link to this article: https://doi.org/10.1080/00295450.2025.2544372

Published online: 19 Nov 2025.

NUCLEAR TECHNOLOGY

DOI: https://doi.org/10.1080/00295450.2025.2544372

Uncertainty and Sensitivity Analysis of the ASTEC Source Term Results of a MBLOCA Scenario with the Activation of Severe Accident Management Actions in a Generic Konvoi Plant

Anastasia Stakhanova [a], Fabrizio Gabrielli [a], Victor Hugo Sanchez Espinoza [a], Eva-Maria Pauli [b], and Axel Hoefer [c]

[a] *Institute of Neutron Physics and Reactor Technology, Karlsruhe Institute of Technology (KIT), Eggenstein-Leopoldshafen, Germany;* [b] *IBEPG (Process and Safety), Framatome GmbH, Erlangen, Germany;* [c] *IBEPG (Process and Safety), Framatome GmbH, Karlstein am Main, Germany*

Received March 12, 2025
Accepted for Publication July 31, 2025

Abstract — *This paper summarizes the joint contribution of Karlsruhe Institute of Technology (KIT)/Framatome GmbH to the HORIZON 2020 MUSA (Management and Uncertainties of Severe Accidents) project, along with additional simulations conducted outside the project focusing on the uncertainty and sensitivity analysis of the Accident Source Term Evaluation Code (ASTEC) results for a medium-break loss-of-coolant accident scenario. This scenario included the activation of severe accident management actions in a generic KONVOI nuclear power plant. The calculation platform used for these analyses is based on the ASTEC code, developed by Autorité de sûreté nucléaire et de radioprotection (ANSR, formerly IRSN) for severe accident simulations, and the KATUSA (KArlsruhe Tool for Uncertainty and Sensitivity Analysis) tool, developed by KIT as part of the KIT/Framatome WAME project. The release of Xe, I, Cs, and Ba to both the containment and the environment was considered as a key figure of merit in the study. The results for the simple statistics, as well as the Spearman correlations between the figure of merit and the selected uncertain input parameters, are presented and discussed. Additionally, an investigation into the failed simulations is provided, along with the option of using a relative timescale.*

Keywords — *ASTEC, severe accident management (SAM), KATUSA, medium-break loss-of-coolant accident (MBLOCA), uncertainty and sensitivity analysis.*

I. INTRODUCTION

The primary objective of the HORIZON 2020 Management and Uncertainties of Severe Accidents (MUSA) project (2019 to 2023) [1], coordinated by CIEMAT, was to assess the capabilities of severe accident (SA) codes in modeling reactor and spent fuel pool accident scenarios for Generation II and III nuclear power plants (NPPs). Specifically, the project aimed to establish a harmonized approach for uncertainty and sensitivity analysis (U&Sa) of the source term (ST) associated with both mitigated and unmitigated SA analyses.

As part of the joint contribution to the MUSA project from the Karlsruhe Institute of Technology (KIT) and Framatome GmbH, a calculation platform was developed at KIT and used in MUSA to perform U&Sa of SA simulation results for a generic KONVOI NPP [2]. The European reference Accident Source Term Evaluation Code (ASTEC) [3], developed by the Autorité de sûreté nucléaire et de radioprotection (ASNR, formerly IRSN), was used to perform the SA analyses. Additionally, the KArlsruhe Tool for

CONTACT Anastasia Stakhanova anastasia.stakhanova@kit.edu

Uncertainty and Sensitivity Analysis (KATUSA) [2], developed by KIT, was used to assess a database of SA simulation results by propagating the uncertainty of selected input parameters and to perform the U&Sa.

KIT's and Framatome's contribution has focused, in particular, on the application of the KATUSA tool to the ASTEC results of three SA scenarios in a generic KONVOI NPP, including a medium-break loss-of-coolant accident (MBLOCA), a MBLOCA scenario in conjunction with a station blackout, and a MBLOCA scenario with the activation of the filtered containment venting system (FCVS) [4,5], as a severe accident management (SAM) action. In addition to fulfilling the main goals of MUSA, KIT and Framatome's contribution also aimed to improve the existing approaches to ST calculations in the context of SA, as well as to quantify the corresponding uncertainties to support the emergency team in making informed decisions [6,7].

This paper is devoted to the U&Sa of the ASTEC results for the MBLOCA SA scenario with the activation of the FCVS simulated up to basemat rupture. Part of these results was initially presented at the ERMSAR-2024 conference in Stockholm [8]. Compared to the conference paper, some additional simulations and analysis have been performed.

The paper is organized in the following way:

1. Sec. II provides a brief overview of the computational framework, including the KATUSA tool, ASTEC KONVOI NPP input, SA scenario description, and uncertain input parameters (UPs). For a more detailed description, see Refs. [2,8].

2. Sec. III summarizes U&Sa results obtained using an absolute timescale for the accident progression.

3. Sec. IV introduces the option of using a relative timescale, and presents the new results of simple statistics and correlation coefficient values from the bigger simulation set (compared to the one presented in the conference paper [8]), which was divided into two subsets by the presence of a filtered venting activation event.

4. Sec. V presents some additional analysis focused on the following:

   a. Influence of excluded failed simulations or outliers on the statistical results.

   b. Influence of the input parameter values on simulation failures.

   c. Influence of the input parameter values on the timing of key events during SA progression.

The list of selected UPs, along with their meanings, probability density functions (PDFs), and references is provided in Table A.1 in the Appendix.

II. COMPUTATIONAL FRAMEWORK

II.A. KATUSA Tool for U&Sa

The KATUSA tool has been developed at KIT in the frame of the KIT/Framatome WAME project [9]. The flowchart of the KATUSA tool consists of the following six modules (see Fig. 1):

1. *Sampling*: The UPs and the corresponding PDFs are provided to the sampling algorithm, which employs either simple random sampling or Latin hypercube sampling. The UPs may be precorrelated. In that case, the sampled values are rearranged according to the correlation matrix calculated using the Iman-Conover method [10,11].

2. *Perform simulations*: A dedicated interface allows for the automatic execution of multiple ASTEC simulations, with each simulation having its own input deck with a corresponding set of sampled uncertain parameter values. Simulations can be run in parallel.

3. *Identify failed simulations*: Failed runs are identified and excluded from further analysis. Information about these simulations (such as when and why did the simulation stop) is collected, allowing the user to investigate the reasons behind the failures;

4. *Collect data from nonfailed simulations*: The results for the selected figure of merit (FoM) from all nonfailed samples are collected and stored in a database. Due to the individual accident progressions in each simulation, the collected results generally have different timescales.

5. *Adjust time grid and interpolate the data*: To prepare the data for U&Sa, the collected data are

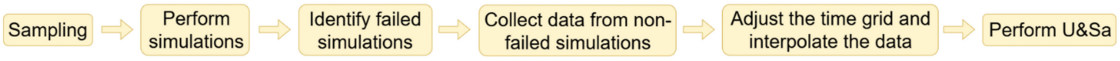

Fig. 1. Flowchart of the KATUSA tool.

interpolated onto a common time grid. The interpolated data are then stored in the database;

6. *Perform U&Sa*: Finally, the U&Sa is performed with the assessed database. For each selected FoM, simple statistics (minimum, mean, maximum, 5th, 50th, and 95th percentiles values), and time-dependent correlation coefficients can be computed.

II.B. ASTEC Model of KONVOI NPP

The core and the containment nodalizations of the ASTEC model are shown in Fig. 2. The core is modeled by means of six cylindrical rings plus two additional channels representing the downcomer and the bypass. Fuel rods, control rods, grid spacers, and plates are considered in each core channel. The containment is modeled by means of 26 rooms plus an auxiliary building. In Fig. 2, the plant (green, red, gray, and light blue boxes), the operating room (white boxes), and the annulus room (light yellow boxes) are shown. The containment and the annulus are connected with each other and with the environment by means of fans (light blue arrows).

Two filtering systems are modeled. The annulus air extraction system (AAES) connects the annulus to the environment and is always available. The efficiency of the AAES filters is 99.995% for aerosols and 99% for gaseous iodine. The FCVS is located on the connection between the containment to the environment, and the efficiency of the filters is 99.9% for aerosols and 99% for gaseous iodine. The FCVS is activated as a SAM action when the absolute pressure in the containment reaches 6.3 bar, and it is deactivated when the absolute pressure in the containment is equal to 3.65 bar. The goal is the containment depressurization, aiming to avoid containment rupture.

All the calculation options were activated in the ASTEC model to consider the main in-vessel and ex-vessel phenomena occurring during the SA scenario from initiation up to the fission product (FP) release to the environment.

Efforts have been spent to properly evaluate the fuel inventory for a typical equilibrium cycle [13]. With this goal, the core has been loaded with 193 fuel assemblies (FAs) composed of 48 U FAs (six batches), 81 U-Gd FAs (six batches), and 64 mixed-oxide FAs (four batches). The ORIGEN depletion code of SCALE 6.2.3 [14] was employed to evaluate a library of fuel inventories, each 30 effective full power days (EFPDs), for a total of 328 EFPDs.

II.C. Uncertain Input Parameters

Eighteen UPs were selected for uncertainty propagation. They, as well as the corresponding PDFs, were selected based on literature review, parametric analyses, and engineering judgment. The full list of the selected UPs and the corresponding PDFs are shown in Table A.1 in the Appendix. The UPs *par1*, *par2*, *par5*, and *par5a* were used to model the FP release simulated by the ASTEC ELSA model. The UPs *par14*, *par15*, and *par16* were used to model the fuel cladding integrity criteria that affects the degradation process in the reactor core.

The UPs *par31* through *par37* are related to the modeling of the behavior of the aerosols in the reactor coolant system and in the containment, which was simulated by the ASTEC SOPHAEROS and CPA calculation models. The

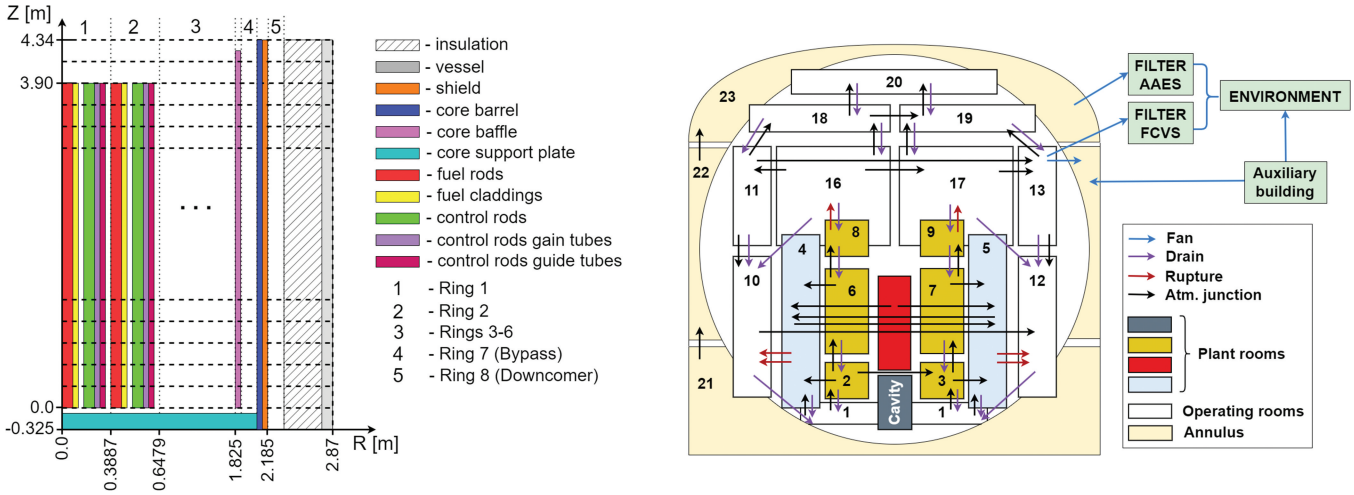

Fig. 2. (left) Core and (right) containment nodalization of the ASTEC model of a generic KONVOI NPP (dimensions not to scale) [12,13].

UP *par41* refers to the uncertainty of the leakage rate from the containment to the annulus. The UP *parBU* refers to the uncertainties of the fuel burnup, namely, the number of EFPDs. Finally, two UPs were considered for characterizing the performance of the FCVS: *parAE* (filter efficiency for aerosols) and *parI2* (filter efficiency for gaseous iodine).

The correlations between the UPs used in the current work are shown in Fig. 3. The correlation coefficients are based on engineering judgment. The employment of a precorrelation matrix aims to improve the correctness of the modeling in the sampling process. As an example, *par34*, *par35*, *par36*, and *par37* are directly precorrelated in Fig. 3, since the minimum particle radius (*par34*) is expected to be directly precorrelated with the maximum particle radius (*par35*). Furthermore, *par34* is directly precorrelated with the shape factor of the particles (*par36* and *par37*).

II.D. Description of the Accident Scenario

The KONVOI plant was assumed to work at full power before the start of the transient. The MBLOCA SA scenario was initiated by a 12-in. break on the cold leg at $t = 0$ s. After the scram signal ($t = 1$ s), admission to the turbine and the main feedwater pumps into the steam generator were closed. Then the conditions for the activation of the emergency core cooling system were fulfilled (at 2.8 s and at 6 s) and the main coolant pumps were coasted down and the pressure regulation in the pressurizer was switched off.

The emergency feedwater system was activated when the liquid level of one steam generator fell below 4.50 m. When the gas temperature in the primary circuit exceeded 650°C, the high- and low-pressure injection systems were activated. The water injections stopped when the tanks were empty, leading to the start of core degradation. When the reactor pressure vessel failed, corium was relocated into the cavity, which was flooded by water when the horizontal erosion reached 0.5 m. As mentioned previously, the FCVS was activated when the absolute pressure reached 6.3 bar, and it was deactivated when the absolute pressure in the containment reached 3.65 bar. The simulation ended when basemat rupture occurred.

III. SUMMARY OF THE PREVIOUS ANALYSIS

In this section, the evaluation results from a set of 300 simulations of the MBLOCA SA scenario with FCVS activation are presented [8]. Of this set, 12 ASTEC simulations, which failed due to convergence problems and other issues, were excluded from the U&Sa. The activation of the FCVS occurred in 48 out of the 300 simulations. Table 1 presents the minimum and maximum values for the occurrence times of the characteristic events.

The maximum and minimum values of the release into the containment and environment for all four considered elements are presented in Figs. 4 and 5. The effect of the venting activation on the release values of Xe and I at the end of the timescale can be observed in the left image in Fig. 4 and in the right image in Fig. 5.

The Spearman correlations between the FP release fraction and UPs are shown in Figs. 6 and 7. For all the considered FPs, the uncertain parameter related to the burnup influenced the containment release. Parameters governing aerosol behaviors are particularly important for Cs and I aerosol releases into the containment, especially in the later stages of the SA progression. The parameter governing the leakage rate affects only the Xe release into the containment. Parameters from the FP release model are important only for the low-volatile elements like Ba.

Note that for correlated UPs, only one parameter from the group is presented; for example, *par1*, *par2*, and *par5a* are correlated. The Spearman correlation values are shown only for *par1* in Fig. 6. Release into the environment is primarily affected by the parameters governing the burnup (*parBU*) and leakage rate (*par41*), with filter efficiency for aerosols (*parAE*) also being important for Cs and I (see Fig. 7).

IV. U&SA NEW RESULTS

In this section, the new results of the U&Sa are presented. Compared to the conference paper, another set of 300 simulations has been added; therefore, in total, 600 simulations were used for analysis. These 600 simulations

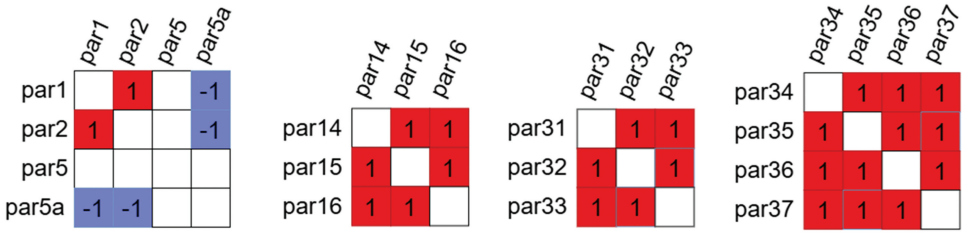

Fig. 3. Precorrelation matrices of the UPs.

TABLE 1

Times of the Characteristic Events During the SA Progression[a]

Event	Minimum (s)	Maximum (s)
Start of FP release from fuel pellets	464.4	684.4
First slump of corium with FP into the lower plenum	734.4	11 884.4
50 tons of corium relocated to the lower plenum	11 784.4	22 946.9
LHVF	3 064.4	29 454.4
Activation of filtered venting	196 245.0	367 073.0
Basemat rupture	187 242.0	402 073.0

[a]For the sample with the shortest time before the lower head vessel failure (LHVF) event, the "50 tons of corium relocated to the lower plenum" event was not detected.

were divided into two subsets: with and without activation of the filtered venting. In addition, anew option of the relative timescale was used to present the results.

IV.A. Relative Timescale Option

Extracting the data for U&Sa in the case using an absolute timescale (which was presented in all our previous works [2,8]) raised several questions, such as how much data are actually used for the U&Sa and how to properly analyze a set of results with very different timings of SA progression.

How the application of an absolute timescale leads to an exclusion of part of the data is illustrated in Fig. 8. For example, if the user wants to perform the U&Sa from the start of FP release up to the basemat rupture, only the data between the latest (among all samples) start of the FP release and the earliest (among all samples) basemat rupture would be used. As a result, part of the data would not be included in the analysis, which is marked in purple in Fig. 8a. While the timing of the start of the FP release does not vary significantly, the timing of basemat rupture can change considerably from, for example, ~1.87×10^5 up to ~4.02×10^5 (see Table 1).

Using the absolute timescale while calculating correlation coefficient values will "mix," for the given time point, the simulations with different states of SA progression; for example, at the given time point t, some of the simulations could already have passed the LHVF event, and some not.

An attempt to overcome these issues was made by introducing the option of a relative timescale in KATUSA. The concept is illustrated in Fig. 8b. For each simulation, its start is treated as time = 0, and its end as time = 1, with all data in between then interpolated onto this timescale and used for the subsequent U&Sa. This approach could be applied not only

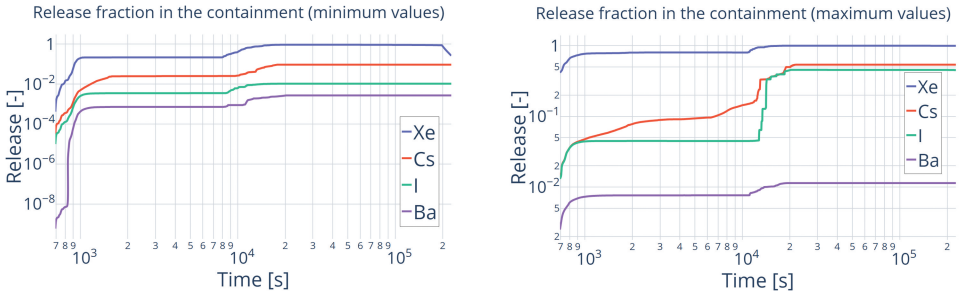

Fig. 4. (left) Minimum and (right) maximum release fractions in the containment for Xe, Cs, I, and Ba.

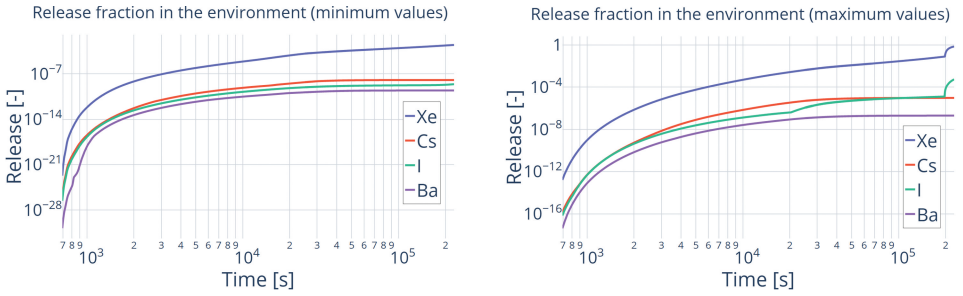

Fig. 5. (left) Minimum and (right) maximum release fractions in the environment for Xe, Cs, I, and Ba.

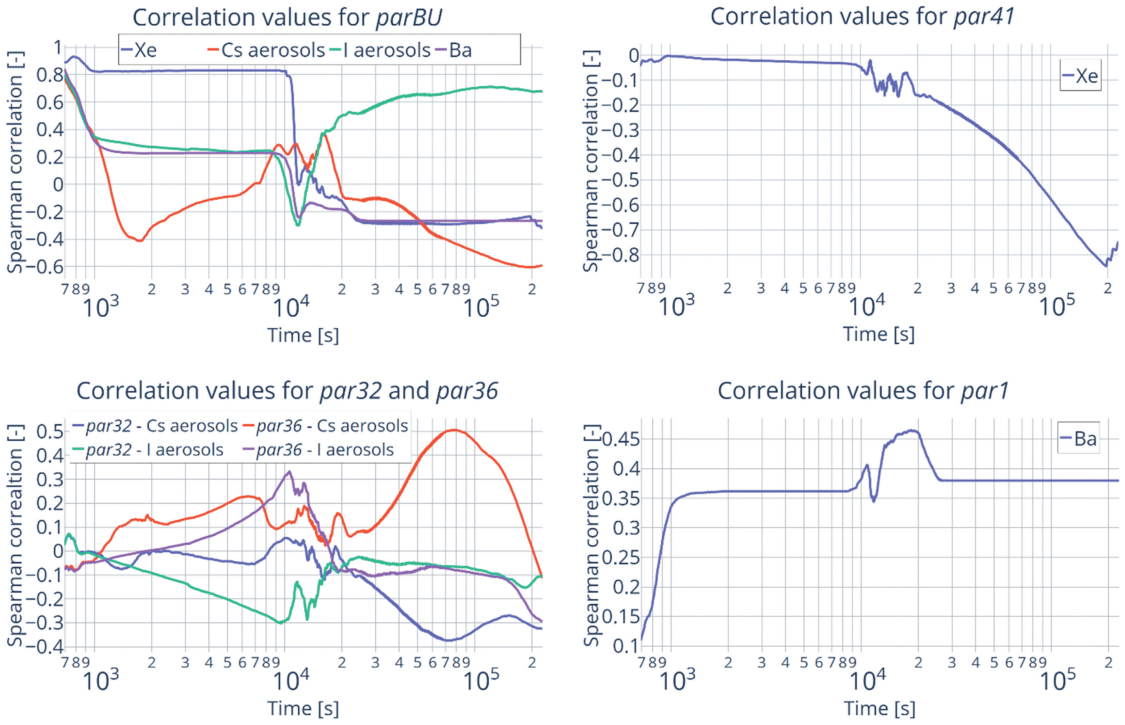

Fig. 6. Spearman correlation values between FP release fraction in the containment and UPs.

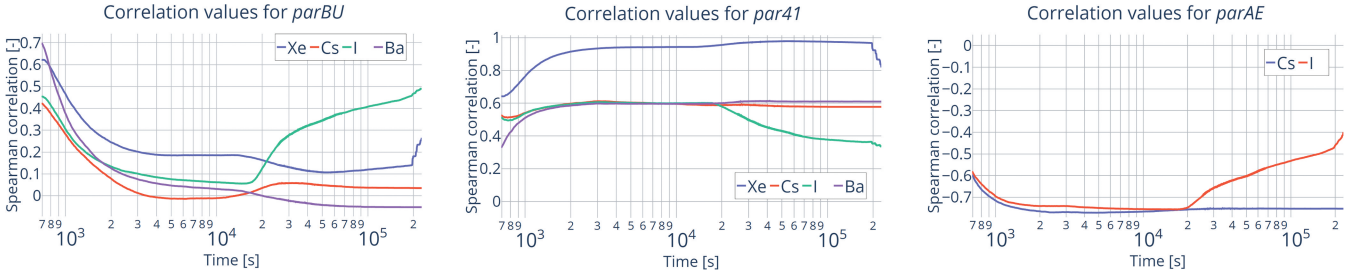

Fig. 7. Spearman correlation values between FP release fraction in the environment and UPs.

to the whole simulation timescale, but to its parts; for example, analyze first the time period between start of FP release and LHVF, and then between LHVF and basemat rupture.

This supposedly allows for focusing on the similar stages between all the considered SA simulations, rather than mixing completely the different states, like in the case of using the absolute timescale. In this work we only generally introduce this idea, as planned for later.

Fig. 9 shows a comparison of the Spearman correlation coefficient values over time obtained using both the absolute and relative timescales. For the correlation coefficient between the release of cesium aerosols into the

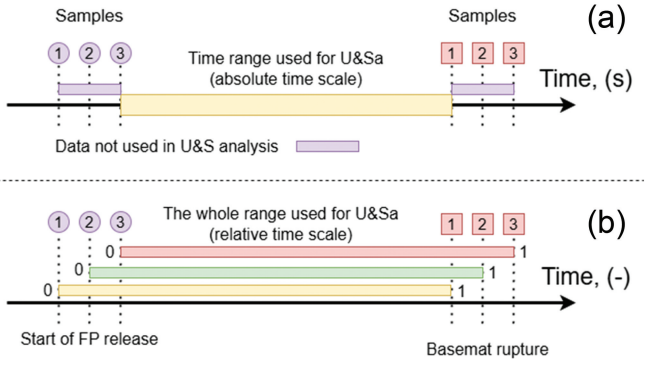

Fig. 8. (a) Absolute and (b) relative timescale options in the KATUSA tool. The parts of the data used in each case for U&Sa are shown.

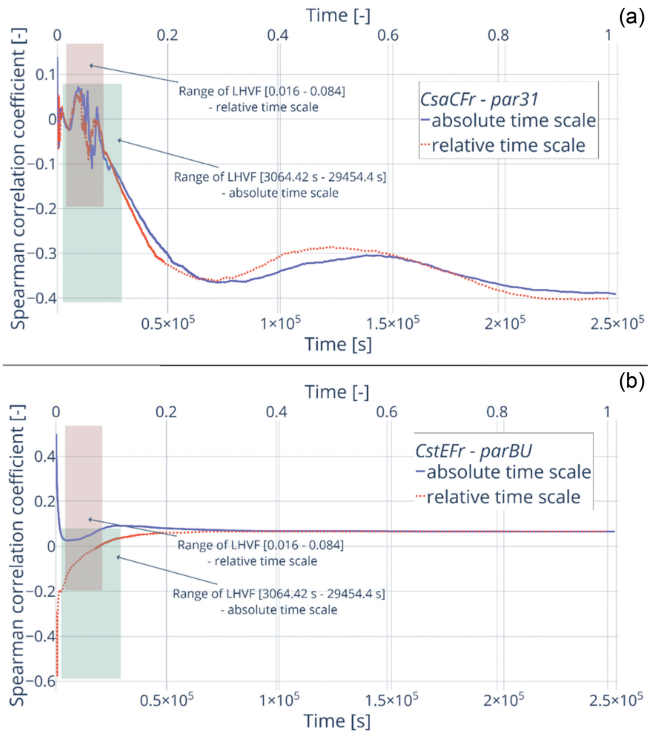

Fig. 9. Comparison of the Spearman correlation coefficient values for two types of timescales: absolute and relative. (a) Correlation between cesium aerosol release into the containment and *par31* and (b) correlation between cesium release into the environment and *parBU*. For both cases, the release values are expressed as a fraction of the initial inventory. The time range during which LHVF occurs is marked with colored rectangles.

containment and the particle mean thermal conductivity (*par31*) (Fig. 9a), changing the timescale from absolute to relative does not result in significant changes in the correlation values.

However, in Fig. 9b, the correlation coefficient between cesium release into the environment and *parBU* shows a notable change at the beginning of the process, depending on which type of timescale is used for the analysis. At the beginning of the process, the release values are very small, making the correlation coefficient quite sensitive to small differences in the release values. The relative timescale option therefore should be investigated more carefully.

IV.B. Simple Statistics Results

This subsection presents the results of the simple statistics analysis. The results are presented for the release of FPs with different volatilities (Xe, Cs, I, and Ba) into the containment and the environment. Data from both simulation sets (300 simulations each) were used for the analysis. The results, which are divided into two subsets, those with and without the activation of filtered venting, are shown on the relative timescale. This division was done for a clearer U&Sa of the simulations with very different release patterns. As will be seen further in the paper, both the simple statistics results and correlation coefficient values were rather different for the two subsets.

The spread of the main event timing across the two simulation sets is presented in Fig. 10. Data for both sets are marked with the same color, as distinguishing between the sets is not necessary. The time of LHVF generally falls between ~18 000 s and 25 400 s (5th percentile = 17947.86 s and 95th percentile = 25349.4 s), while the time of the basemat rupture occurs between ~240 000 s and 329 000 s (5th percentile = 239754.0 s and 95th percentile = 328571.1 s). Two distinctive outliers, which are significantly lower than the 5th percentile values, are marked in Fig. 10 with colored rectangles.

In the left image in Fig. 11, the timing of the switch to the filtered venting is presented for both data sets. Out of the total 600 simulations, this event occurred in 97 (48 and 49 for each set, respectively). From the left image in Fig. 11, it can be observed that around half of the samples with filtered venting activation were located below even the 5th percentile of the basemat rupture time, while the other half were between the 5th and 95th percentile values of the basemat rupture time. This raised the question of how many samples with earlier basemat rupture times should be excluded when using an absolute timescale, highlighting the potential usefulness of the relative timescale option.

Additionally, the dependency of the filtered venting activation time on the burnup value (uncertain parameter *parBU*) is shown in the right image in Fig. 11. The Pearson and Spearman correlation values were −0.687 and −0.552, respectively (see also Table 2 in Sec. V.C Influence of UPs on the timing of key events during SA progression). Sequences with higher burnup values exhibited a faster core degradation due to the higher amount of FPs in the fuel. This led to a larger release of FPs from the fuel and their transport to the containment, which caused a faster pressure increase, and consequently, an earlier activation of the venting system.

Fig. 12 illustrates the xenon release into the environment for all the considered simulations divided into two subsets: without venting activation in the left image in Fig. 12 and with activated venting in the right image in Fig. 12. It can be observed that the maximum release values with activated venting at the end of the SA were almost ~8 × higher.

The simple statistics results for the release of xenon, cesium, iodine and barium into the containment and the environment are presented on Figs. 13 through 16. These

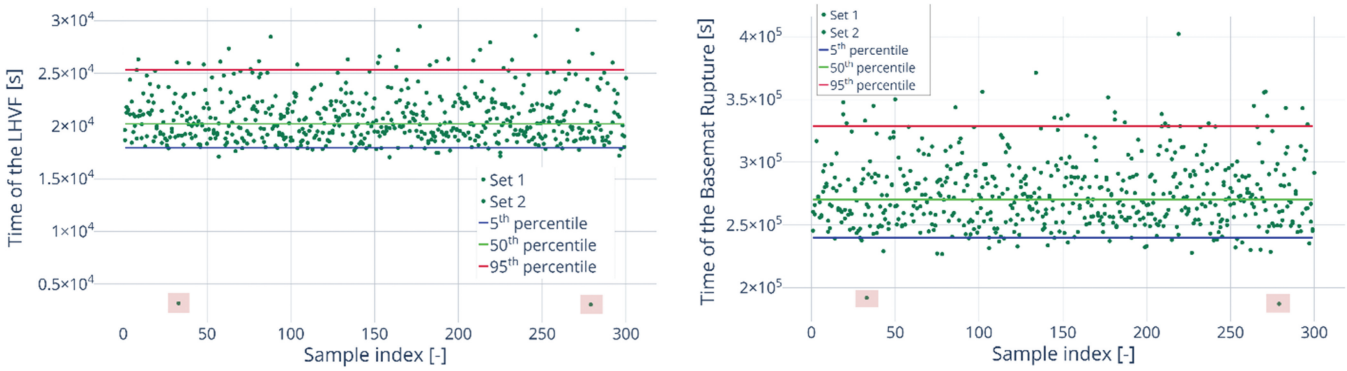

Fig. 10. Timing of the main events for all samples for both simulation sets: (left) LHVF and (right) basemat rupture. Percentiles are marked with lines. Two distinctive outliers that are below the 5th percentile value are marked with a rectangle.

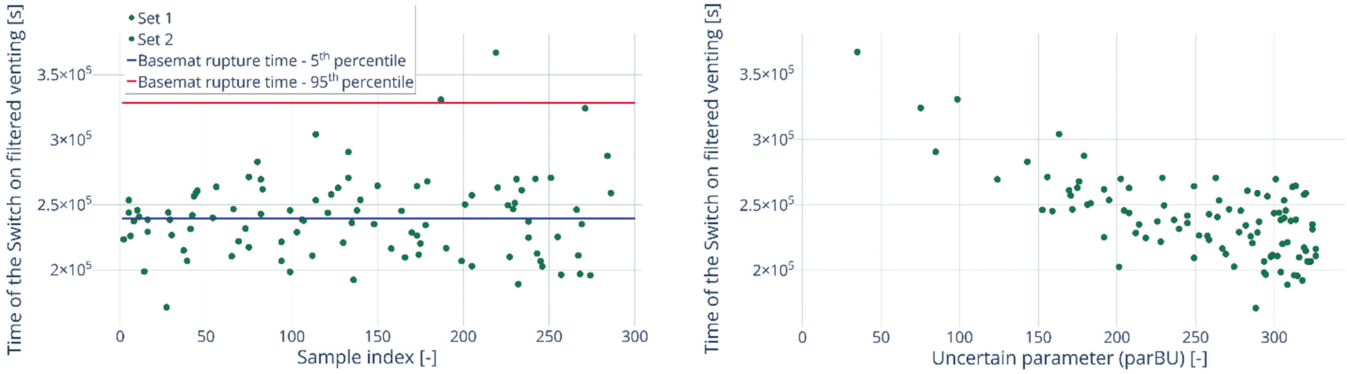

Fig. 11. Results from the simulations with the switch to filtered venting: (left) time of the switch to the filtered venting for both simulation sets and (5th and 95th percentile values of the basemat rupture time are marked with blue and red lines, respectively.

results are shown on the relative timescale to cover all cases with activated filtered venting. The results for two subsets (with and without activation of the filtered venting) are marked differently in the figures.

The simple statistics for the total amount of Xe in the containment and the environment are shown in Fig. 13. The activation of the FCVS occurred in 97 samples out of 600, and the effect of this SAM action is clearly visible in the results. It is important to note that in the MBLOCA + SAM ASTEC data set, the AAES was also activated from the beginning of the transient.

The median value of the amount of Xe in the containment at the end of the SA was about 90% of the initial Xe inventory for cases without filtering and about 35% for cases with filtering. The maximum amount of Xe released into the environment for cases with filtering activation could reach approximately 80% of the initial amount of Xe, while without filtering, the maximum value was around 12%.

The results for the total mass of I in the containment and the environment are shown in Fig. 14. The median value of the mass fraction in the containment was approximately 3% for the subset without filtering and around 33% for subset with activated filtering. The maximum values for the two subsets were at approximately 40% and 45%, respectively. For the environment, the filtering effect was also evident. The maximum total amount of iodine released was about 0.1% of the initial

TABLE 2

Pearson and Spearman Correlation Coefficient Values Between the Timing of Key Events During SA Progression and the UP Related to Burnup (*parBU*)

Event	Pearson Correlation	Spearman Correlation
Start of FP release from the fuel pellets	−0.775	−0.920
First slump of corium with FP into the lower plenum	−0.498	−0.684
LHVF	−0.387	−0.410
Switch on filtered venting	−0.687	−0.552
Basemat rupture	−0.728	−0.754

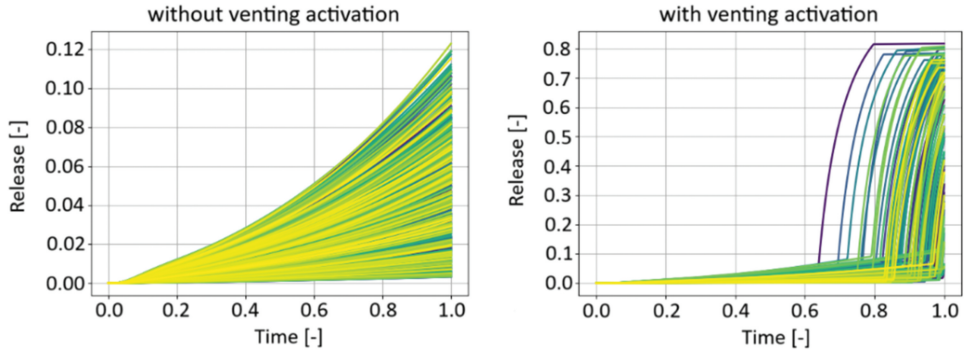

Fig. 12. Xenon release (as fraction of the initial inventory) into the environment over time (relative timescale): (left) without venting activation and (right) with venting activation.

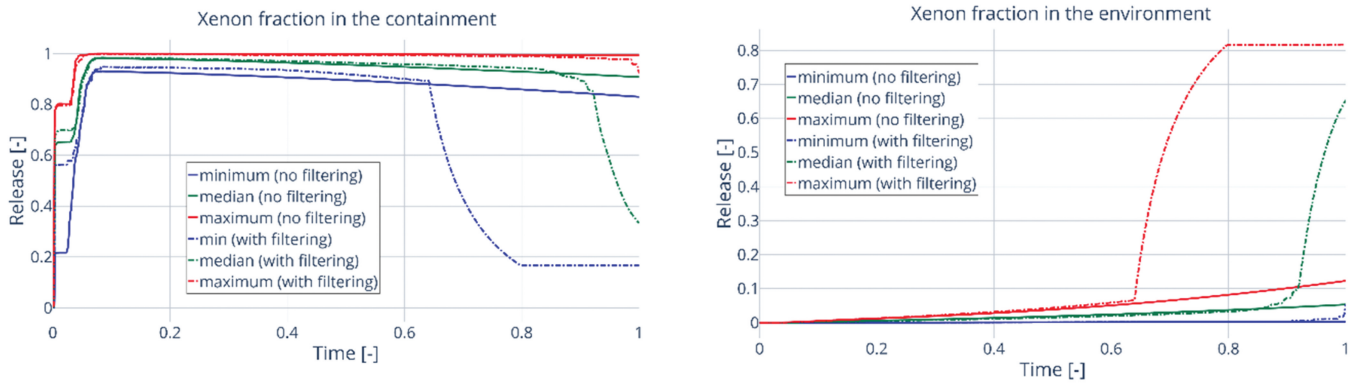

Fig. 13. Simple statistics of (left) the mass of Xe in the containment and (right the environment as fraction of the total amount in the initial core loading.

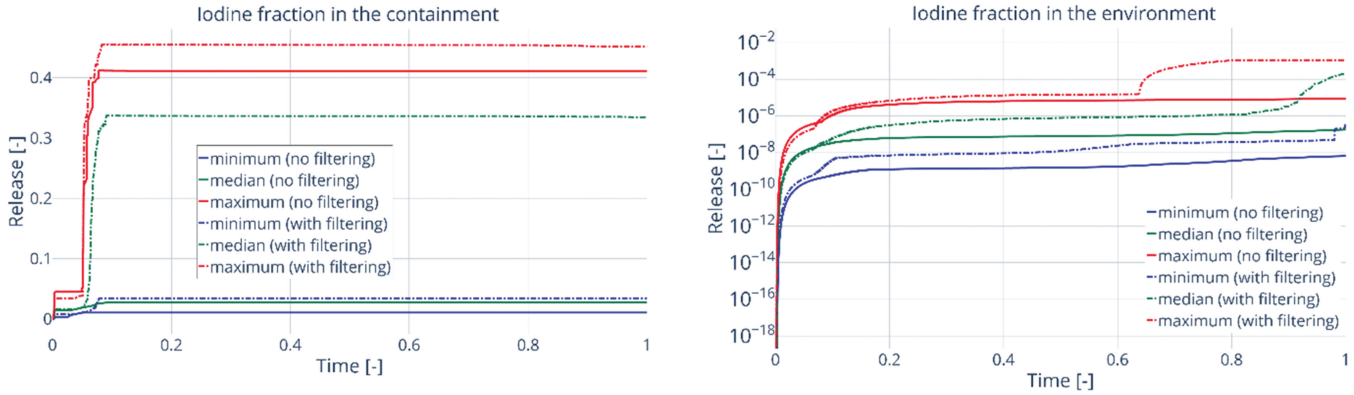

Fig. 14. Simple statistics of (left) the mass of I in the containment and (right) the environment as fraction of the total amount in the initial core loading.

inventory for the subset with filtering and 1×10^{-3}% for the subset without filtering.

The results for the total mass of Cs in the containment and the environment are shown in Fig. 15. While the filtering effect for Cs is not as clearly visible as for Xe and I, the results are presented for the entire set of 600 simulations. The median mass fraction in the containment was about 32%, with the maximum value about 55%. For the environment, the median and maximum values were about 8×10^{-5}% and 10^{-3}% of the initial inventory, respectively.

The results for the total mass of Ba in the containment and the environment are shown in Fig. 16. Similar to Cs, the

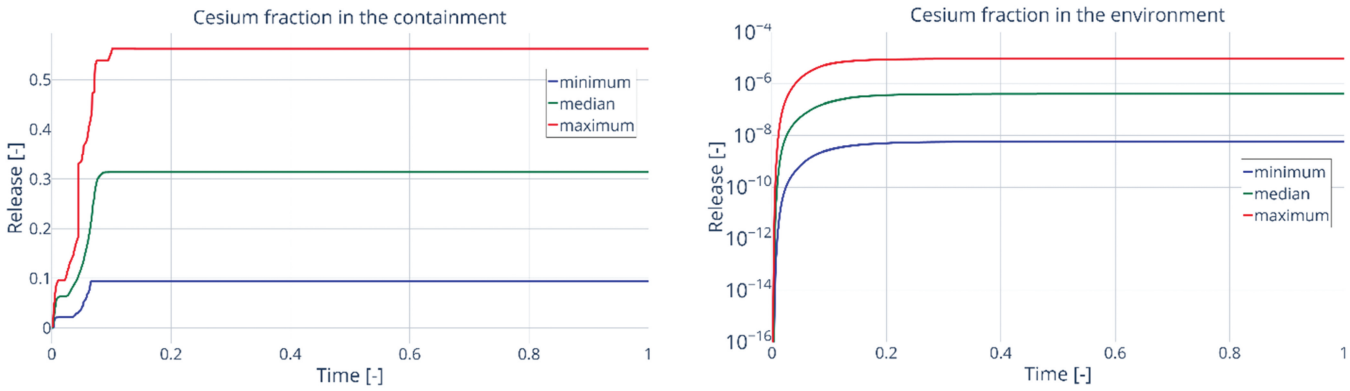

Fig. 15. Simple statistics of (left) the mass of Cs in the containment and (right) the environment as fraction of the total amount in the initial core loading.

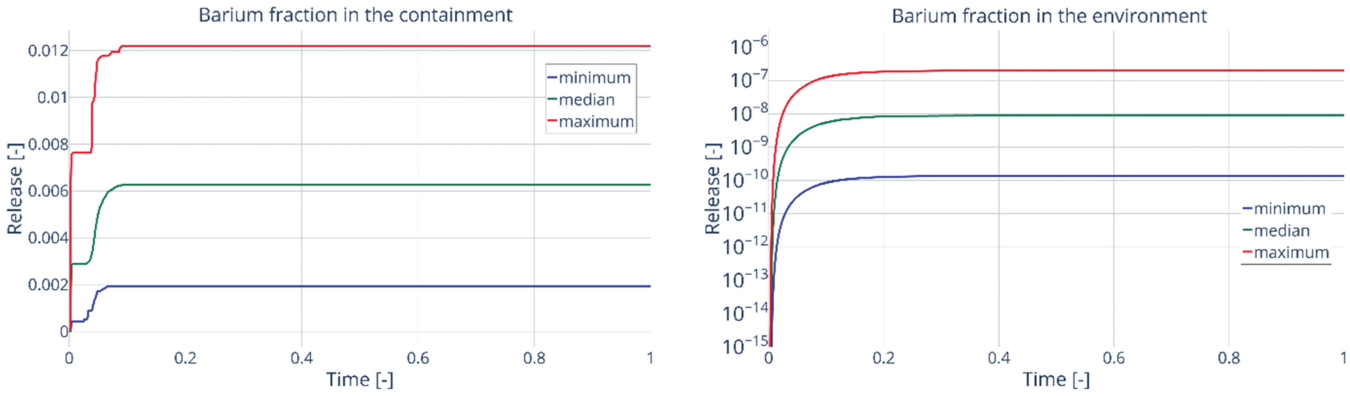

Fig. 16. Simple statistics of (left) the mass of Ba in the containment and (right) the environment as fraction of the total amount in the initial core loading.

results are presented for all 600 simulations without dividing the data into subsets. The mass fraction released to the containment was about 0.6% for the median value and about 1.2% for the maximum value. For the environment, the median and maximum values were around 1×10^{-6}% and 2×10^{-5}% of the initial inventory, respectively.

IV.C. U&Sa Results

This section presents the Spearman correlation values between the UPs and the selected FoMs. The Spearman correlation was used in this work due to the assumed nonlinearity and monotonicity of the relationship between the UPs and FoMs. Only the results involving correlations greater than 30% are shown. All the results are presented on the absolute timescale due to the issues mentioned in Sec. IV.A. The subsets with and without activation of the filtered venting are analyzed separately.

The Spearman correlation coefficients for the release of Xe to the containment and the environment (as a fraction of the initial mass in the core) are shown in Fig. 17. The results indicated that the parameters *parBU* (fuel burnup) and *par41* (containment leakage) had the most significant impact on these FoMs. For the release to the containment, *parBU* showed a strong correlation (about 80%) during the in-vessel phase of the scenario, while the correlation with *par41* was negative, reaching −80%, indicating that higher containment leakage led to more Xe being released to the environment.

It is important to note that the correlation of *par41* with the release to the environment decreased when the FCVS was activated at around 180 000 s (see left image in Fig. 17, subset with FCVS activation). This was the result of the sudden, massive release triggered by the activation of the FCVS. Regarding the release to the environment, the correlation of *par41* remained close to 1 for a significant portion of the process, but decreased toward the end for the subset with FCVS activation. The correlation with *parBU* remained relatively constant at around 0.25 throughout most of the SA progression and increased near the end for the subset of simulations with activated filtered venting.

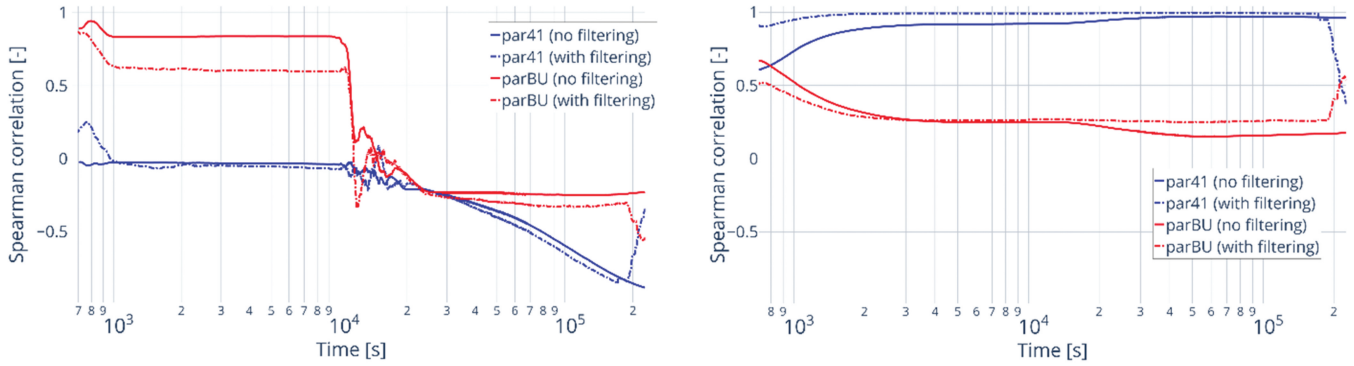

Fig. 17. Spearman correlations between the dominant UPs and the mass fraction of the initial loading of Xe (left) in the containment and (right) in the environment.

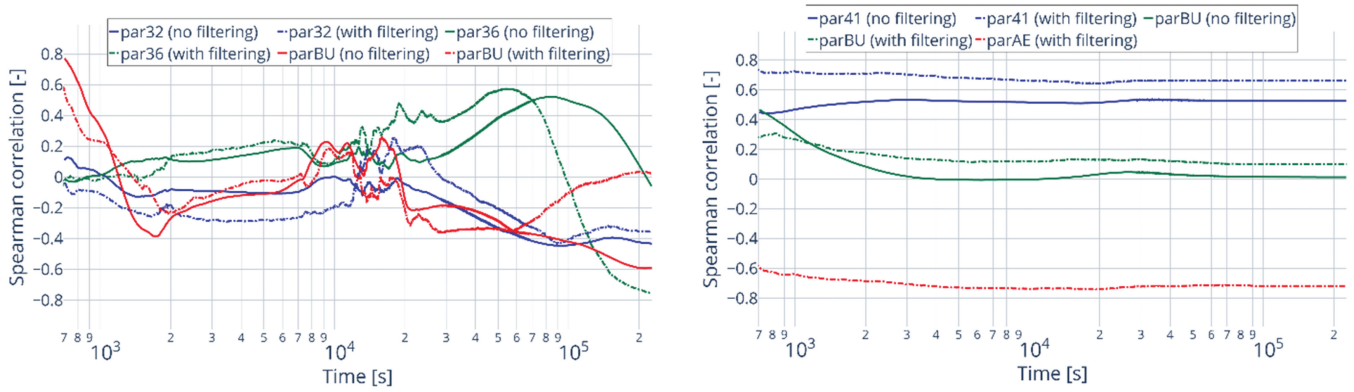

Fig. 18. Spearman correlations between the dominant UPs and the mass fraction of the (left) initial loading of Cs aerosols in the containment and (right) Cs released into the environment.

The Spearman correlations for cesium aerosols in the containment and cesium release into the environment are shown in Fig. 18. Regarding the aerosols in the containment, correlation coefficients greater than 30% were observed for the UPs related to the fuel burnup (*parBU*), thermal properties (*par31*, *par32*, and *par33*), geometry (*par34* and *par35*), and aerosol behavior (*par36* and *par37*).

Due to the correlation between the parameters (see Fig. 3), only the values for *par32* and *par36* are shown. These correlations were particularly notable after the flooding of the cavity (around 50 000 s). The correlations related to *parBU* ranged from 30% to 40% during the in-vessel phase of the scenario, becoming between −30% and −60% after cavity flooding (for the subset without filtering). The correlations for the aerosol thermal properties (*par31*, *par32*, and *par33*) were approximately −30% around the time of cavity flooding (for the subset without filtering).

As shown in Fig. 18, from this point onward, correlations for *par34* through *par37* became significant, reaching ~50% at around 75 000 s for both subsets. The differences between the results with and without filtering activation were substantial for *par34 through par37* throughout most of the process, starting from 10 000 s. This difference could affect the decision on whether to consider the UP as significant for the given stage of the SA. The influence of *parBU* after the cavity flooding was highly pronounced for both subsets, with the curves moving in opposite directions.

Regarding the release to the environment, significant correlations were observed for the UPs related to containment leakage (*par41*) and filter efficiency for aerosols (*parAE*). Specifically, the Spearman correlation for *par41* was approximately 55% for the subset without filtering and 65% to 70% for subset with filtering. Meanwhile, the correlation for *parAE* was negative, with a value of about −75% during the transient. The effect of *parBU* was evident only at the very start of the process, and this effect was more pronounced for the subset without filtering.

The time-dependent behavior of the Spearman correlations for iodine aerosols in the containment is shown in the left image in Fig. 19. The same parameters that mostly

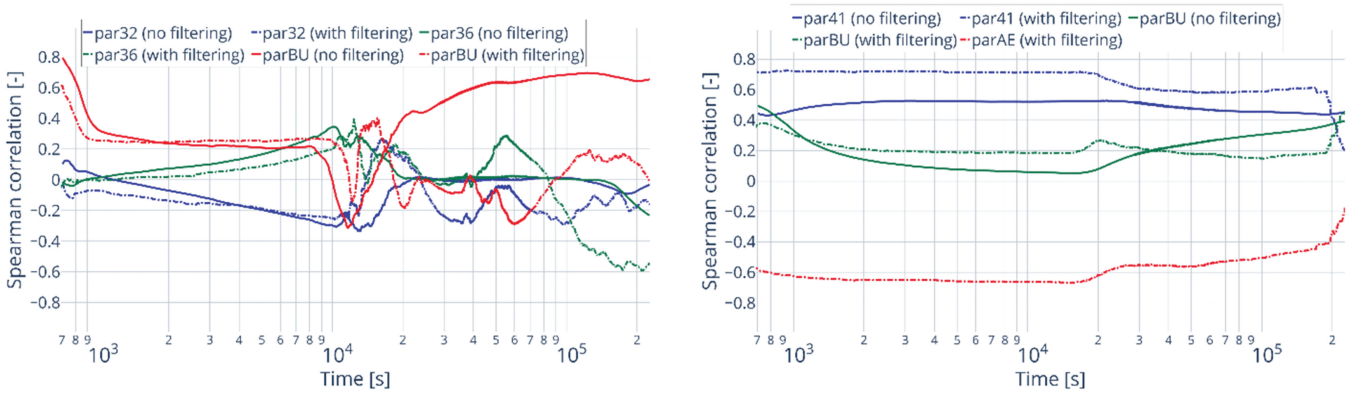

Fig. 19. Spearman correlations between the dominant UPs and the mass fraction of the initial loading of (left) iodine aerosols in the containment and (right) iodine released into the environment.

influenced the release of Cs aerosols, fuel burnup (*parBU*), thermal properties (*par31*, *par32*, and *par33*), geometry (*par34* and *par35*), and aerosol behavior (*par36* and *par37*), also impacted the iodine aerosols. As for the Cs aerosols, due to the correlations between the parameters (see Fig. 3), only the values for *par32* and *par36* are shown here. The correlation for *parBU*, starting at ~15 000 s, significantly differed between for the two subsets: those with and without filtered venting.

For the cases without filtered venting, the correlation was much higher, reaching around 70% by the end of the process, compared to near 0% for cases with filtered venting. The correlations for *par31*, *par32*, and *par33* also showed significant differences between the two subsets. At around 15 000 s, the correlation value was approximately 20% for the subset with filtered venting and −30% for the subset without filtered venting. Additionally, the correlations for *par34* through *pa37* showed major differences between the two subsets starting at around 40 000 s and continuing until the end of the SA process.

The Spearman correlations for the release of iodine to the environment are shown in the right image in Fig. 19. The results indicated that the fuel burnup (*parBU*) and the containment leakage (*par41*) significantly affected the FoM. As with the previous results, a noticeable difference between the subsets with and without filtered venting was observed. For *par41*, the correlation remained around 50% for the subset without filtered venting and increased to 65% to 70% for the subset with filtered venting.

A similar difference of approximately 10% to 15% was seen for *parBU*. A sharp change in the correlation values for both *par41* and *parBU* occurred at the very end of the process for the subset with filtered venting. Additionally, the results highlighted a strong correlation between the efficiency of the filters for aerosols (*parAE*) and the FoM. For this parameter, the Spearman correlation was about −65% during the in-vessel phase due to the employment of the AAES, decreasing up to −20% at the end of the process.

The results of the sensitivity analysis for the release of barium to the containment and the environment are shown in Fig. 20. The results were not divided into subsets due to barium's relatively low volatility, which made filtering irrelevant. Due to this lower volatility, the selected UPs related to the ASTEC model for the release from the fuel showed significant correlations with the release to the containment (left image in Fig. 20).

Specifically, the FoM exhibited a noticeable positive correlation of around 40% with the properties of the fuel grains (*par1* and *par2*) during the scenario. Due to the correlation between parameters (see Fig. 3), only the values for *par1* are shown. The correlation with fuel burnup (*parBU*) was significant immediately after the start of FP release from the fuel, but it quickly decreased to around 20% during the first 1000 s of the transient.

The release of barium to the environment (right image in Fig. 20) showed a strong correlation with the containment leakage (*par41*), reaching approximately 60% for most of the SA progression. As with the containment, the correlation with fuel burnup (*parBU*) was significant only at the beginning of the process, rapidly decreasing within the first 1000 s.

V. FAILED SIMULATIONS AND TIMING OF KEY EVENTS: ADDITIONAL ANALYSIS

In this section, various questions are addressed, like the following:

1. How and whether exclusion of the failed simulation can influence the results of the U&Sa?

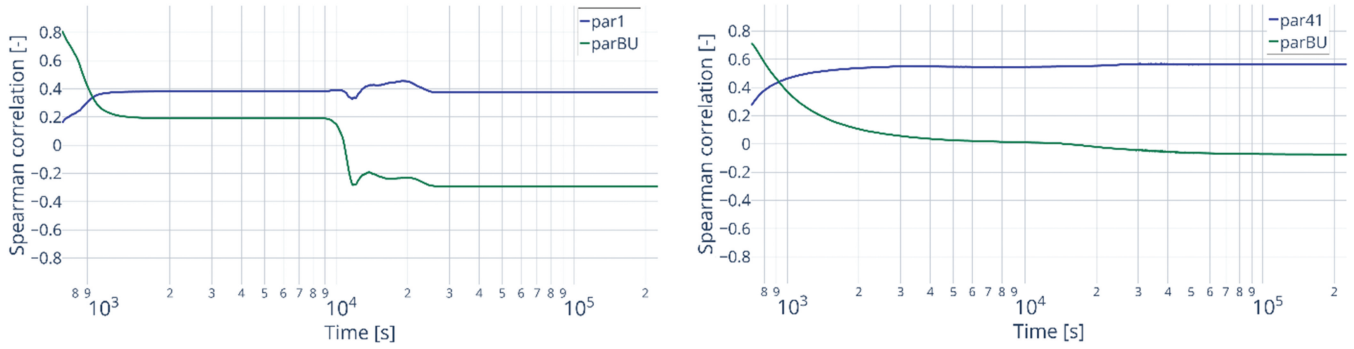

Fig. 20. Spearman correlations between the dominant UPs and the mass fraction of the initial loading of Ba released into (left) the containment and (right) the environment.

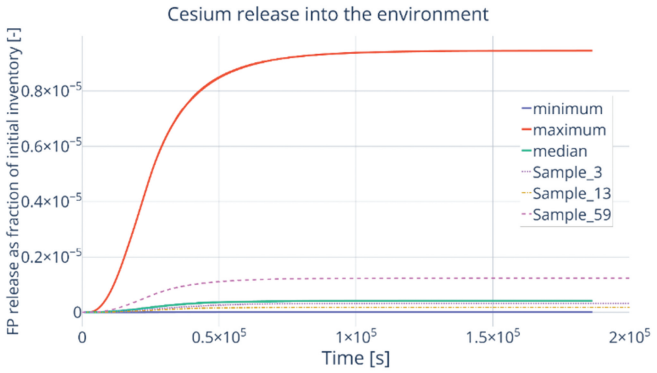

Fig. 21. Cesium release (as a fraction of the initial inventory) into the environment. Simple statistics for correctly completed simulations and data for three failed simulations.

2. The same question as the previous one, but for the simulations with shorter SA progression times, which should be excluded from analysis in the case using the absolute timescale?

3. Are UPs values affecting simulation failure?

4. How are UPs values affecting the timing of the key events during the SA progression?

Questions 3 and 4 are included as one of the postprocessing options in the KATUSA tool, while questions 1 and 2 currently require separate analysis. It should be useful to address these questions in any U&Sa.

V.A. Exclusion of Failing and Outlying Simulations

Some of the simulations in the set may fail for various reasons, and these samples are automatically excluded during the "Collect data from non-failed simulations" step in the KATUSA tool workflow (see Fig. 1 and Sec. II.A. for a more detailed description). Additionally, in the input file for this step, the user can specify the indexes of any other samples to exclude, such as simulations with accident progressions that are either too short or too long compared to the rest of the set.

A logical question arises: How do excluded simulations affect the results of simple statistics and U&Sa? In the current version of KATUSA, there is no automatic procedure for addressing this, so this section presents an attempt to show where the values from the failed simulations fall within the range of values from successfully completed simulations.

For illustration, one set out of two is used here. In this set, the following samples failed: 3, 13, 59, 87, 237, 274, 288, 290, 291, 294, 297, and 300. Although the data for sample 291 were lost, the other failed samples provided sufficient data for illustration. Fig. 21 shows the simple statistics (minimum, median, and maximum values) over time for cesium release into the environment (as a fraction of the initial inventory) for the subset of successfully completed samples. The release values for a couple of the failed samples are also presented. It can be observed that none of the three presented failed samples fall outside the release range of the correctly completed simulations.

The maximum release value (reached at the end of the process) among all correctly finished simulations in this set was 9.46×10^{-6} (with all release values presented as a fraction of the initial inventory). The maximum values of release reached at the end of the SA for the other failed samples did not exceed 1.67×10^{-6}. In the same way, the user can check whether the values from the failed samples exceeded the range of values from the nonfailed samples for any other FoM. Simulation failures typically occur due to some convergence issues, and output results are available up to a certain point in time.

As mentioned previously, in addition to the failed samples, the user can exclude other samples, such as those with accident progressions that are too fast

Fig. 22. Defining the time range for further U&Sa in the KATUSA tool. The figure shows three samples with different timings of SA progression.

compared to the rest of the simulation set. This is necessary due to how the data extraction and further postprocessing are organized within the KATUSA tool. Fig. 22 illustrates that, among three simulations with different SA progression timings, only the data between the maximum time of one event (in this case, the start of FP release) and the minimum time of the other event (in this case, basemat rupture) will be considered for further analysis. As a result, samples with too short SA progression times are typically discarded, which could potentially influence the results. In such cases, the user can perform the same check as for the failed cases to assess their impact.

The possibility of adding a more detailed automatic check for the influence of sample exclusion into the KATUSA tool is being considered. In the two sets of simulations presented, only one sample from each set showed a significantly shortened SA progression, and this did not result in any visible changes to the results.

V.B. Correlation Between UP Values and Simulation Failure

Out of the two simulation sets (600 simulations in total, with 300 simulations in each set), 26 simulations failed (14 in one set and 12 in the other). A check was conducted to determine whether the values of the UPs corresponding to the failed cases formed any cluster in the space of the sampled input parameters. The results are presented on Fig. 23. In the one-dimensional projection of the parameter space, no clear evidence of a cluster of failed cases was found.

For the two most influential input parameters, *par41* and *parBU* (see Table A.1 in the Appendix for more information about UPs), it can be seen that slightly more failed cases appeared in the upper half of the plot for *par41*, with more failed cases falling within the range [15; 30] than in [0; 15], and for *parBU*, more failed cases were found in the range [150; 300] than in [0; 150]. However, in both cases, the differences were not substantial enough to suggest any clear pattern.

V.C. Influence of UPs on the Timing of Key Events During SA Progression

This subsection presents the results of an investigation into how the selected UPs influenced the SA progression, specifically the timing of key events, such as LHVF, basemat rupture, and others.

The timing of each key event was plotted against the UP value, and both Pearson and Spearman correlation coefficients were calculated for each pair of event timing and UP. For most of the pairs, both correlation coefficients were negligible, falling within the range [−0.15; 0.15]. More significant correlation values were found only for parameter related to burnup (*parBU*), as shown in Table 2. Fig. 24 presents this correlation in the form of a scatter plot for two selected events. The results showed that higher burnup values led to an earlier start of FP release and generally faster SA progression.

VI. CONCLUSIONS

This study assessed the database of SA simulation results for a MBLOCA scenario employing the FCVS SAM action for a generic KONVOI NPP. One set of simulations was conducted as part of the KIT/Framatome joint contribution to the HORIZON MUSA project, coordinated by CIEMAT, while the second set and the introduction of the relative timescale were carried out outside the MUSA project. All simulations were performed using the ASTEC code, developed by ASNR (formerly IRSN), and U&Sa was carried out using the KATUSA tool, developed at KIT under the KIT/Framatome WAME project [6,7].

The primary focus of this work was on the propagation of the uncertainty in 18 ASTEC input parameters and its effect on the ST, specifically the release of Xe, I, Cs, and Ba to both the containment and the environment. The uncertainty of each parameter was characterized using lower and upper limits, as well as PDFs derived from open literature and engineering judgment. Simple statistics and Spearman correlation coefficients were computed to assess these effects. The results were divided into two subsets: one with and one without the activation of the filtered venting system. The correlation coefficients were calculated separately for both subsets.

The analysis revealed that for both subsets, the release to the containment was primarily influenced by the containment leakage (only for Xe), burnup (Xe, I, Cs, and Ba), the parameters related to the properties

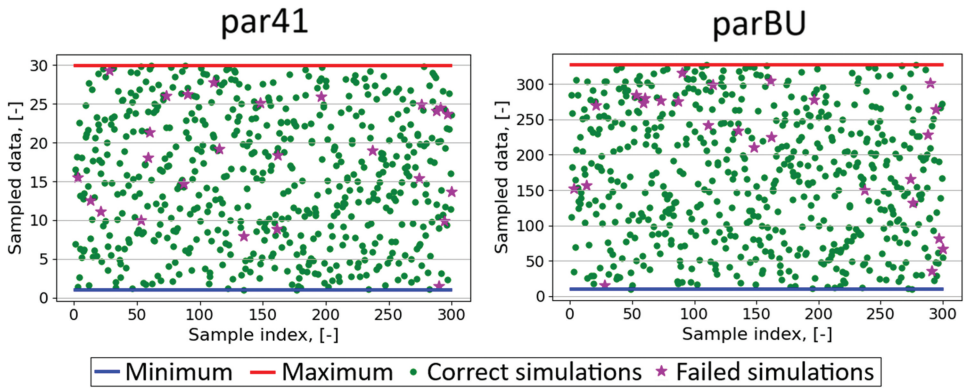

Fig. 23. Values of UPs with highlighted failed cases for both simulation sets: (left) *par41* and (right) *parBU*.

and the behavior of the aerosols (I and Cs aerosols), and the parameters related to the FP release model (only for Ba). The release to the environment was mainly influenced by containment leakage and fuel burnup (for Xe, I, Cs, and Ba). The FCVS system filter efficiency affected the release of I and Cs aerosols into the environment (in the subset with activated filtered venting). Additionally, certain differences in the correlation were observed between cases with and without filtered venting activation, particularly regarding the impact of burnup and aerosol-related parameters on the release of I and Cs aerosols to the containment.

The introduction of the relative timescale option provided a solution to the problem of discarding simulations with atypical progression times from the analysis. While this option requires further investigation, valuable insights were gained by applying it to the U&Sa.

The investigation also addressed the potential influence of failed simulations on the U&Sa and examined the impact of UPs values on the simulation failure. The analysis showed that failed simulations did not affect the U&Sa results and could be safely excluded from further analysis. Furthermore, UP values did not have a direct impact on the simulation failure.

Last, the influence of UP values on the SA progression, specifically the timing of key events, such as the start of FP release, LHVF, and basemat rupture, was investigated. Among all the selected parameters, only burnup had a clear effect on the SA progression.

In summary, a substantial amount of ASTEC simulation data was collected by KIT/Framatome within the MUSA project for scenarios with FCVS activation. The results of the U&Sa identified the main parameters affecting the ST, providing a foundation for further analyses of scenarios involving SAM actions.

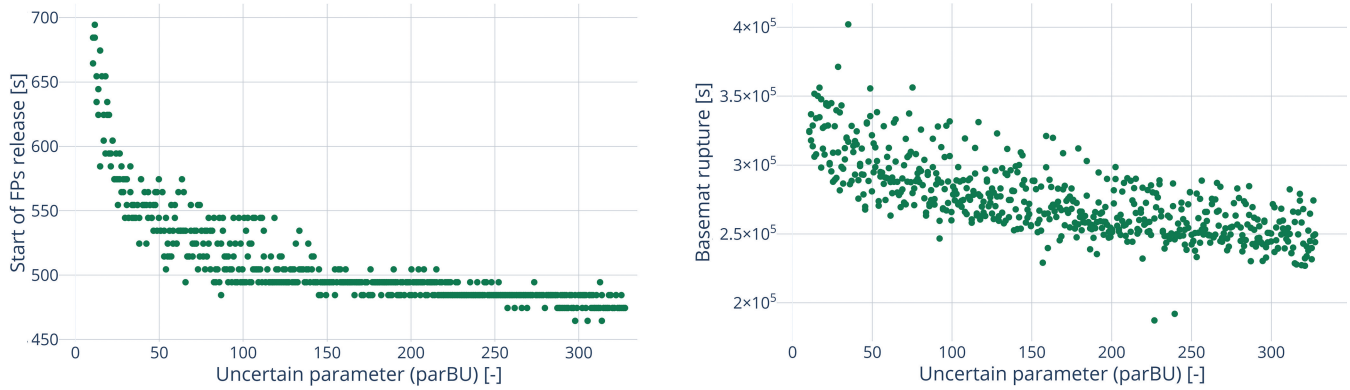

Fig. 24. Timing of the key events for all samples from both simulation sets plotted against the value of the UP: (left) start of FP release versus *parBU* and (right) time of basemat rupture versus *parBU*.

APPENDIX A

In Table A.1 the detailed information about the selected uncertain input parameters is provided, including their description, chosen probability density functions and references to the literature.

TABLE A.1

UPs: Meaning, PDFs, and References

UP	PDF	PDF Parameters	Description	Reference
par1	Normal	$\mu = 5.0$, $\sigma = 30\%$	Correction factor for the ratio surface/volume (S/V) of the fuel pellets due to roughness	[15–17]
par2	Normal	$\mu = 0.03$, $\sigma = 30\%$	Correction factor for the ratio S/V of the fuel pellets for the limited steam access	[15–17]
par5	Normal	$\mu = 1.2E\text{-}5$, $\sigma = 30\%$	Geometrical diameter of the grain	[18,19]
par5a	Triangular	Mode = 2.0E-6, minimum = 1.6E-6 maximum = 3.4E-6	Standard deviation of geometrical diameter of the grain	[18,19]
par14	Normal	$\mu = 2500.0$, $\sigma = 10\%$	Threshold Temperature of the cladding dislocation (K)	[20,21]
par15	Normal	$\mu = 2300.0$, $\sigma = 10\%$	Threshold Temperature of the oxide layer dislocation (K)	[22]
par16	Normal	$\mu = 250.0E\text{-}4$, $\sigma = 20\%$	Threshold thickness of the oxide layer (mm)	[22]
par31	Uniform	Minimum = 2.975, maximum = 4.025	Particle mean thermal conductivity (J/m/K)	Engineering judgment
par32	Uniform	Minimum = 714.0, maxium = 966.0	Average specific heat (J/kg K) of the aerosol	Engineering judgment
par33	Triangular	Mode = 3000.0, minimum = 2610.0, maximum = 10 000.0	Particle mean density (kg/m^3)	[23]
par34	Triangular	Mode = 1.1E-8, minimum = 1.0E-8, maxm = 2.0E-07	Particle minimum geometrical radius (m)	[24]
par35	Triangular	Mode = 1.99E-5, minimum = 5.0E-6, maximum = 2.0E-5	Particle maximum geometrical radius (m)	[24]
par36	Triangular	Mode = 1.0, minimum = 0.9, maximum = 1.0	Shape factor relative to particle coagulation	[23]
par37	Beta	$\alpha = 1.0$, $\beta = 5.0$, minm = 1.0, maximum = 3.0	Shape factor relative to Stokes velocity	[21]
par41	Uniform	Minimum = 1.0, maximum = 30.0	Coefficient for the leakage rate between containment and annulus	Engineering judgment
parBU	Uniform	Minimum = 10.0, maximum = 328.0	EFPDs	Engineering judgment
parAE	Truncated log-normal	Minimum = 0.9, maximum = 0.9995	Filter efficiency for aerosols	Truncated log-normal
parI2	Truncated log-normal	Minimum = 0.9, maximum = 0.999	Filter efficiency for gases (I_2)	Truncated log-normal

Acknowledgment

This paper reflects only the authors' views. The European Commission is not responsible for any use that may be made of the information this paper contains.

Author Contributions

CRediT: **Anastasia Stakhanova:** Conceptualization, Data curation, Formal analysis, Investigation, Methodology, Software, Validation, Visualization, Writing – original draft; **Fabrizio Gabrielli:** Conceptualization, Funding acquisition, Investigation, Methodology, Project administration, Supervision, Writing – review & editing; **Victor Hugo Sanchez Espinoza:** Funding acquisition, Project administration, Supervision, Writing – review & editing; **Eva-Maria Pauli:** Methodology, Writing – review & editing; **Axel Hoefer:** Methodology, Writing – review & editing.

Disclosure Statement

No potential conflict of interest was reported by the author(s).

Funding

This project received funding from the Euratom research and training programme 2014-2018 under grant agreement [no. 847441].

ORCID

Anastasia Stakhanova http://orcid.org/0000-0001-6192-0001

References

1. L. E. Herranz et al., "The EC MUSA Project on Management and Uncertainty of Severe Accidents: Main Pillars and Status," *Energies*, **14**, *4473*, 1 (2021); https://doi.org/10.3390/en14154473.
2. A. Stakhanova et al., "Uncertainty and Sensitivity Analysis of the ASTEC Simulations Results of a MBLOCA Scenario in a Generic KONVOI Plant Using the FSTC Tool," *Ann. Nucl. Energy*, **192**, 109964 (2023); https://doi.org/10.1016/j.anucene.2023.109964.
3. P. Chatelard and L. Laborde, "ASTEC V2. 2 Code Validation: Illustrative Results and Main Outcomes," *Nucl. Eng. Des.*, **413**, 112547 (2023); https://doi.org/10.1016/j.nucengdes.2023.112547.
4. S. Galushin et al., "Source Term Uncertainty Analysis of Filtered Containment Venting Scenarios in Nordic BWR," *Ann. Nucl. Energy*, **218**, 111406 (2025); https://doi.org/10.1016/j.anucene.2025.111406.
5. L. S. Lebel et al., "Severe Accident Consequence Mitigation by Filtered Containment Venting at Canadian Nuclear Power Plants," *Ann. Nucl. Energy*, **102**, 297 (2017); https://doi.org/10.1016/j.anucene.2016.08.005.
6. A. Stakhanova et al., "Application of the MOCABA Algorithm and the FSTC Tool for Source Term Predictions During Severe Accident Scenarios," *Ann. Nucl. Energy*, **184**, 109703 (2023); https://doi.org/10.1016/j.anucene.2023.109703.
7. E. Pauli et al., "Prediction of the Radiological Consequences of a Severe Accident Scenario in a Generic KONVOI Nuclear Power Plant," *Proc. ERMSAR2022*, Paper 311, p. 338, Karlsruhe, Germany, May 16–19, 2022 (2022).
8. A. Stakhanova et al., "Uncertainty and Sensitivity Analysis of the ASTEC Source Term Results of a MBLOCA Scenario with the Activation of Severe Accident Management Actions in a Generic KONVOI Plant," *Proc. ERMSAR2024*, Paper 001, p. 695, Stockholm, Sweden, May 13–16, 2024 (2022).
9. "Strategy for Competence Building and the Development of Future Talent for Nuclear Safety" Federal Ministry for Economic Affairs and Energy, Berlin, Germany (2020); https://www.bundeswirtschaftsministerium.de/Redaktion/EN/Publikationen/Energie/strategy-for-competence-building-and-the-development-of-future-talent-for-nuclear-safety.pdf?__blob=publicationFile&v=1.
10. R. L. Iman and W. J. Conover, "A Distribution-Free Approach to Inducing Rank Correlation Among Input Variables," *Commun. Stat. Simul. Comput.*, **11**, *3*, 311 (1982); https://doi.org/10.1080/03610918208812265.
11. S. C. Maree, "Correcting Non Positive Definite Correlation Matrices," BSc Thesis, Department of Applied Mathematics, Delft University of Technology (2012).
12. I. G. García-Toraño, "Further Development of Severe Accident Management Strategies for a German PWR Konvoi Plant Based on the European Severe Accident Code ASTEC," Dr. -Ing, Dissertation, Karlsruher Institut für Technologie, Fakultät für Maschinenbau (2017).
13. F. Gabrielli et al., "Impact of Realistic Fuel Inventories on the Radiological Consequences of a Severe Accident Scenario in a Generic Konvoi Plant by Means of the ASTEC Code," *Proc. KERNTECHNIK*, Leipzig, Germany, June 21–22, 2022.
14. "SCALE: A Comprehensive Modeling and Simulation Suite for Nuclear Safety Analysis and Design," ORNL/TM-2005/39, Version 6.2.3, Oak Ridge National Laboratory (2022).
15. T. Ikeda et al., "Analysis of Core Degradation and Fission Products Release in Phebus FPT1 Test at IRSN by Detailed Severe Accidents Analysis Code, IMPACT/SAMPSON," *Nucl. Sci. Technol.*, **40**, *8*, 591 (2003).

16. G. Brillant, C. Marchetto, and W. Plumecocq, "Fission Product Release from Nuclear Fuel I. Physical Modelling in the ASTEC Code," *Ann. Nucl. Energy*, **61**, 88 (2013); https://doi.org/10.1016/j.anucene.2013.03.022.

17. G. Brillant, C. Marchetto, and W. Plumecocq, "Fission Product Release from Nuclear Fuel II. Validation of ASTEC/ELSA on Analytical and Large-Scale Experiments," *Ann. Nucl. Energy*, **61**, 96 (2013); https://doi.org/10.1016/j.anucene.2013.03.045.

18. G. Pastore et al., "Uncertainty and Sensitivity Analysis of Fission Gas Behavior in Engineering-Scale Fuel Modelling," *J. Nucl. Mater.*, **456**, 398 (2015); https://doi.org/10.1016/j.jnucmat.2014.09.077.

19. K. W. Song et al., "Sintering of Mixed UO_2 and U_3O_8 Powder Compacts," *J. Nucl. Mater.*, **277**, *2–3*, 123 (2000); https://doi.org/10.1016/S0022-3115(99)00212-3.

20. Y. Pontillon et al., "Lessons Learnt from VERCORS Tests: Study of the Active Role Played by UO_2–ZrO_2–FP Interactions on Irradiated Fuel Collapse Temperature," *J. Nucl. Mater.*, **344**, *1–3*, 265 (2005); https://doi.org/10.1016/j.jnucmat.2005.04.053.

21. "State-of-the-Art Reactor Consequence Analyses (SOARCA) Project: Sequoyah Integrated Deterministic and Uncertainty Analyses," NUREG/CR-7245, U.S. Nuclear Regulatory Commission (2018).

22. P. Hofmann et al., "ZrO_2 Dissolution by Molten Zircaloy and Cladding Oxide Shell Failure. New Experimental Results and Modelling," FZKA 6383, Forschungszentrum Karlsruhe1999).

23. "State-of-the-Art Reactor Consequence Analyses Project: Uncertainty Analysis of the Unmitigated Long-Term Station Blackout of the Peach Bottom Atomic Power Station," NUREG/CR-7155, SAND2012-10702P, U.S. Nuclear Regulatory Commission (2012).

24. J. C. Helton et al., "Uncertainty and Sensitivity Analysis of a Model for Multicomponent Aerosol Dynamics," *Nucl. Technol.*, **73**, *3*, 320 (1986); https://doi.org/10.13182/NT86-A16075.